

# USArray design implications for wavefield imaging in the lithosphere and upper mantle

ALAN LEVANDER, Rice University, Houston, Texas, U.S.

Although seismic tomography is currently the mainstay of global seismic imaging, the large-scale deployment of portable instruments to be conducted as the USArray component of Earthscope over the next decade will allow much higher resolution imaging of the solid earth using migration/inversion methods similar to those used in petroleum exploration. Direct wavefield imaging in solid earth structural seismology has been uncommon in comparison to practices in exploration seismology, generally due to the large separation between seismic stations. With the development of portable observatory quality broadband (0.01-20 Hz) seismographs and acquisition of modest numbers of them for the PASSCAL instrument pool over the past decade, a number of academic field programs have had receiver spacing dense enough for wavefield back-projection and imaging. Recordings from these experiments have been used in several different imaging schemes, all of which are outgrowths of and bear resemblance to either post- or prestack depth migration, or migration-inversion, of the Kirchhoff, plane-wave, or Belkyn-Burridge formulations (e.g., Bostock et al., 2001; Poppeliers and Pavlis, 2003; and by Pavlis and by Aster and Wilson in this issue).

Four hundred of these instruments will be deployed as USArray, a coarse array that will sweep across the United States over a 10-year period. This array, known as the Transportable Array, and informally referred to as "Bigfoot," will begin in Southern California and expand north to the Canadian border. When fully deployed, USArray, extending along the western United States from Canada to Mexico, will begin moving eastward to the Atlantic seaboard, before transfer to Alaska and Hawaii. Within Bigfoot will be denser "Flexible" component arrays targeting specific crust and upper mantle structures. The scale of USArray is enormous: At full deployment Bigfoot will cover approximately 2 000 000 km<sup>2</sup>, with an instrument spacing of 70 km. The denser, embedded passive arrays of the Flexible Array will have instruments spaced in the range of 10-20 km.

The waves from earthquakes used for the most common form of direct imaging are at source-receiver offsets of 30-100° along the globe, equivalent to ~3300-11 000 km. Moderate- to large-sized earthquakes (mb > 5.0) at this range produce P-waves with frequencies in the 0.3-3 Hz and the 0.02-0.1 Hz bands. A broad peak in the earth's background seismic radiation, largely ocean-generated, often contaminates the 0.15-0.2 Hz band.

**Structural imaging.** Many different phases within the earthquake wave train are potentially useful for structural imaging. Here I describe a commonly used method that isolates P-to-S-wave conversions under a receiver array from the direct P-wave. Direct P is the first arrival from the earthquake source, and at many distances is well separated from other later arriving phases, making it a relatively simple input on the receiver end of the raypath (Figure 1). At each interface or perturbation the input P field generates a forward scattered P-wave and a converted, forward scattered S-wave. The converted S phases are useful for estimating the interface and perturbation structure of the earth beneath the receiver array. Broadband seismograph stations record three components of ground motion. If the vertical motion is considered largely due

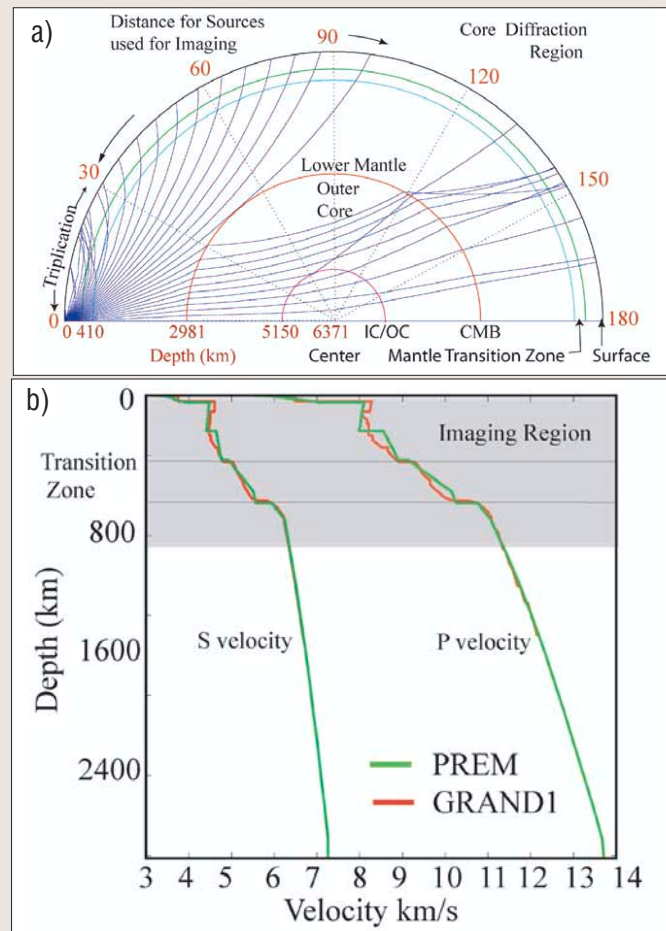


**Figure 1.** (a) Raypaths for compressional waves through the PREM model. Imaging with receiver functions is normally done at the receiver end with signals arriving from 30 to ~100° on the globe to avoid complications in the direct wave arising from upper mantle and core-mantle boundary structures. CMB is core mantle boundary; IC/OC is inner core-outer core boundary. (b) PREM (Dziewonski and Anderson, 1981) and Grand and Helmborgers' (1984) Shield North America 1D velocity models from the surface to the core-mantle boundary at 2981 km depth.

to P motions and the horizontal radial component is considered largely composed of converted S-waves, then deconvolving the vertical component of motion from the radial yields a spiked time series in which the earthquake source signature has been removed (the direct P pulse) and consists of spiked direct P- followed by S-wave conversions. In practice the deconvolution is improved with a number of modifications developed in the exploration industry, including applying a zero-phase shaping filter, using recordings of the same source at multiple nearby stations to estimate the average source wavelet, and adding white noise to the deconvolution operator to stabilize it. The receiver function can also be improved by rotating the vertical and radial components into the longitudinal (incident ray direction) and orthogonal radial (orthogonal to ray direction) components before deconvolution. Generally, deconvolved time series from earthquakes from the same source region are summed to produce an average receiver response. The resulting time series is known as

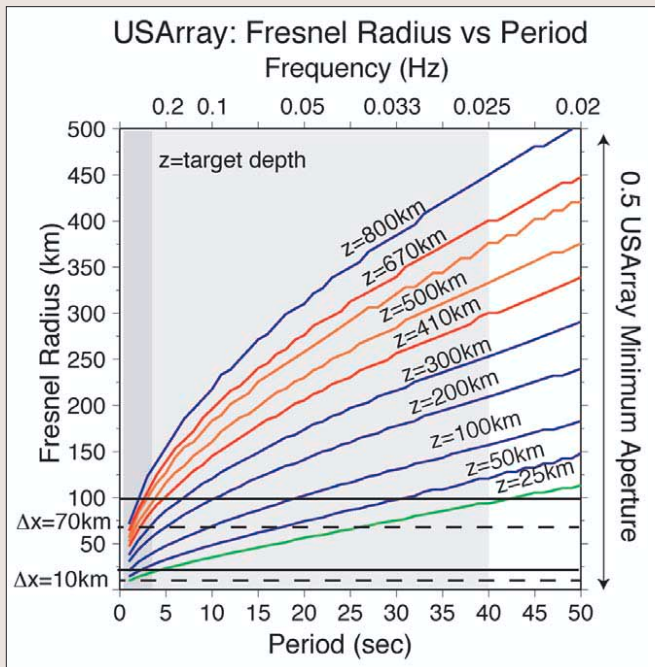


**Figure 2.** Fresnel zone radius versus period parameterized by depth. Each curve corresponds to the Fresnel zone radius as a function of period for a given depth. The curves are color coded according to depth in the earth, with the crust green, and the mantle transition zone red. The first Fresnel zone must be adequately sampled in the Fourier sense for image reconstruction. The diagram shows at what depth the Fresnel zone will be adequately sampled at a given period for the Transportable and Flexible arrays (solid black lines). Here I assume a linear Flexible array deployment with station increment 10 km. The Transportable array is 2-D with 70 km station increment. The diagonal sampling is ~40% denser than along the array lattice directions.

a receiver function and has been widely used to investigate the layered structure of the lower crust and upper mantle. Calculating receiver functions reduces a vector problem to a scalar problem and produces an approximately accurate representation of the converted shear-wave field.

Receiver functions at multiple stations and from multiple sources can be processed and interpreted in a variety of ways. Some investigators use a method analogous to normal move-out correction and stacking, although for multiple station receiver functions this is a far less straightforward procedure than for the exploration case.

A very simple and physically correct means to process the data is to back propagate the wavefield in a manner analogous to prestack shot-gather depth migration: All receiver functions from a single earthquake are depth migrated, all earthquakes are migrated, and the image volumes of all earthquakes are stacked. The imaging condition is that the recording time, relative to the earthquake origin time, is set equal to the sum of (1) the traveltime of direct P to a scattering point and (2) the traveltime of a scattered S from that point to the surface recorder. The back propagation and imaging can be done with one of various forms of the scalar Kirchhoff integral (see Appendix).

**Background velocity model and imaging considerations.** In practice the P-wave traveltimes and geometrical spreading amplitudes are calculated from the source region to the imaging region (Figure 1a), using an appropriate 1D velocity model for the path. A number of well known averaged 1D velocity models for the earth or for different tectonic regions of the continents have been developed, e.g. PREM (Dziewonski and Anderson, 1981) or one of Grand and Helmborgers' (1984) 1D velocity models for North America. An appropriate 1D earth

model predicts velocity within the earth reasonably well. Within the imaging region (Figure 1b), P and S traveltimes and amplitudes are calculated using a local upper mantle velocity model that can be laterally as well as vertically variable, taking into account velocity anomalies identified by body wave tomography.

Generally receiver functions are made with earthquake waves arriving from distances of 30-100°. This avoids multiple arrivals in the direct P-wave field at distances less than 30° resulting from the triplications caused by the rapid velocity increase in the upper mantle transition zone, and complications at distances greater than 100° resulting from the diffraction from the core-mantle boundary (Figure 1a).

The back projection of waves for image reconstruction requires adequate spatial sampling of the first Fresnel zone of a scattered wave by the receiving array. Figure 2 shows the size of the Fresnel zone as a function of wave period (reciprocal frequency) parameterized by depth. This figure illustrates the imaging capabilities for the USArray Bigfoot and Flexible arrays at different depths in the earth for different periods in the PREM reference model. The 2D Bigfoot array will record spatially unaliased signals at 20 s period and greater (< 0.05 Hz) from scatterers at and below 100 km depth, and signals at 10 s period and greater (< 0.1 Hz) from scatterers below 200 km. The array is poorly suited for image formation at the shallower depths corresponding to most of the continental lithosphere using higher frequencies due to spatial aliasing. Receiver functions from Bigfoot can still provide interface depths, but the information on lateral structural variability made possible by migrating surface seismic data will be lost. To overcome this limitation of the Bigfoot array, deployments of the Flexible array with station spacing of 10 km will permit imaging with the highest frequencies normally recorded from teleseismic distances (0.3-3.0 Hz) for most of the lithosphere (depths at and greater than ~25 km depth, corresponding to the middle of the continental crust).

**Synthetic test cases.** Figure 3 shows synthetic seismograms for a series of point scatterers (converters) at different depths in the PREM 1D reference model, and their reconstructions. I examined two linear array (2D) cases, one corresponding to the spatial sampling of the Transportable Array and one to that of a 2D Flexible Array deployment. For the synthetics and reconstructions, scattering was assumed isotropic and reconstructions were made using the imaging algorithm outlined above, with the point scatterers beneath the center of the array. In the absence of the direct P-wave signal and perfect knowledge of the velocity model, the synthetics and reconstructions confirm the inferences of Figure 2, showing the depths and frequencies at which image degradation occurs for each array resulting from inadequate spatial sampling and signal interference.

Because earthquake sources are not distributed uniformly over the globe, it will be common that most signals arriving from distant events at the USArray stations will arrive from a small number of azimuths. Since the input signal originates from a laterally distant source, it provides an imaging geometry skewed to the source side that I illustrate with a synthetic example (Figure 4). Here I have used an array configuration similar to a real field experiment described in the next session, including station dropouts in the array configuration. Receiver spacing is approximately that of the Bigfoot array. A number of seismic horizons are depicted, including three short converters beneath the left end of the array at lithospheric depths, and three semicontinuous converters corresponding to the base of the lithosphere at 200-250 km depth, and the two rapid velocity increases at transition zone depths. The syn-

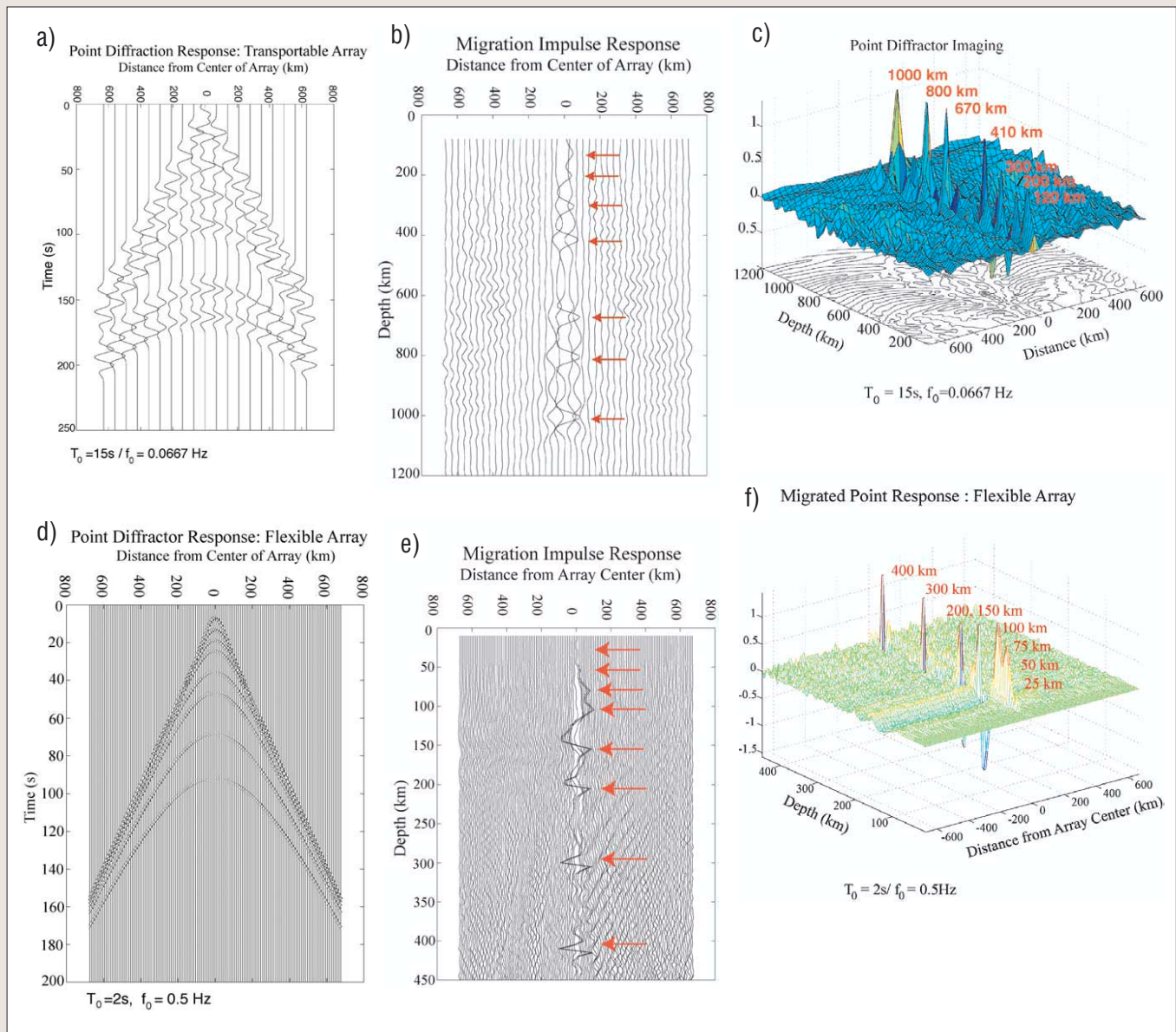


**Figure 3.** Point converter receiver function (i.e., converted S-wave) response and reconstructions for 1330-km linear arrays with (a-c) 70-km station spacing, and (d-f) 10-km station spacing. The former has a center frequency of 0.0667 Hz, the latter 0.5 Hz. (b-c) Migrated impulse response of receiver functions from (a). With 70-km station interval, events shallower than about 200 km are not well reconstructed in the low-frequency band, whereas deeper events are. (e-f) In the high frequency band with 10-km station spacing, point scatterers are reconstructed at depths as shallow as 25 km, and are well resolved at 75 km depth and greater.

thetic seismogram is shown in Figure 4b and the reconstruction in Figure 4c. The shallowest converter in the lithosphere is poorly imaged, even though it is well positioned beneath the array for image reconstruction, due to the Fresnel zone sampling and signal interference with the next deeper converter. The next two converters are reasonably well imaged with some interference. The lateral variability in the three deeper horizons are reasonably well imaged but are incomplete due to the image region being skewed to the source side. As target depth increases the imaging region moves toward the source by over 200 km. Structure in the center of the model at 600-700 km depth is fully imaged, whereas structure directly above it at 200-250 km depth is not. Similarly the right edge of the imaging region moves sourceward by a similar amount, truncating the converters.

**MOMA experiment data.** The Missouri to Massachusetts seismic experiment (MOMA) was a linear array of 18 portable broadband seismographs deployed over ~1748 km between

IRIS Global Seismic Network stations Cathedral Cave Missouri (CCM) and Harvard (HRV) in Massachusetts (Fischer et al., 1996). The average station spacing was 83 km, comparable to the station interval planned for the Bigfoot component of USArray. MOMA was at the southern edge of the North American craton, the interior core of the North American continent that has relatively high seismic velocities in the upper mantle. Receiver functions were computed by Li et al. (2000). The earthquake sources used for receiver functions were distributed around the array from three azimuths. Here I have used the simplest possible assumptions, adopting a similar 1D velocity structure for all three azimuths, a 1D structure in the upper mantle, and isotropic conversion coefficients. (The conversion coefficients are in fact strongly angle dependent.) Differences in predicted and observed arrival times of the direct P-wave were treated as static corrections and generally had a weak linear trend superimposed on a small dc component. The direct P-wave was muted prior to migration. No dip filtering was applied.

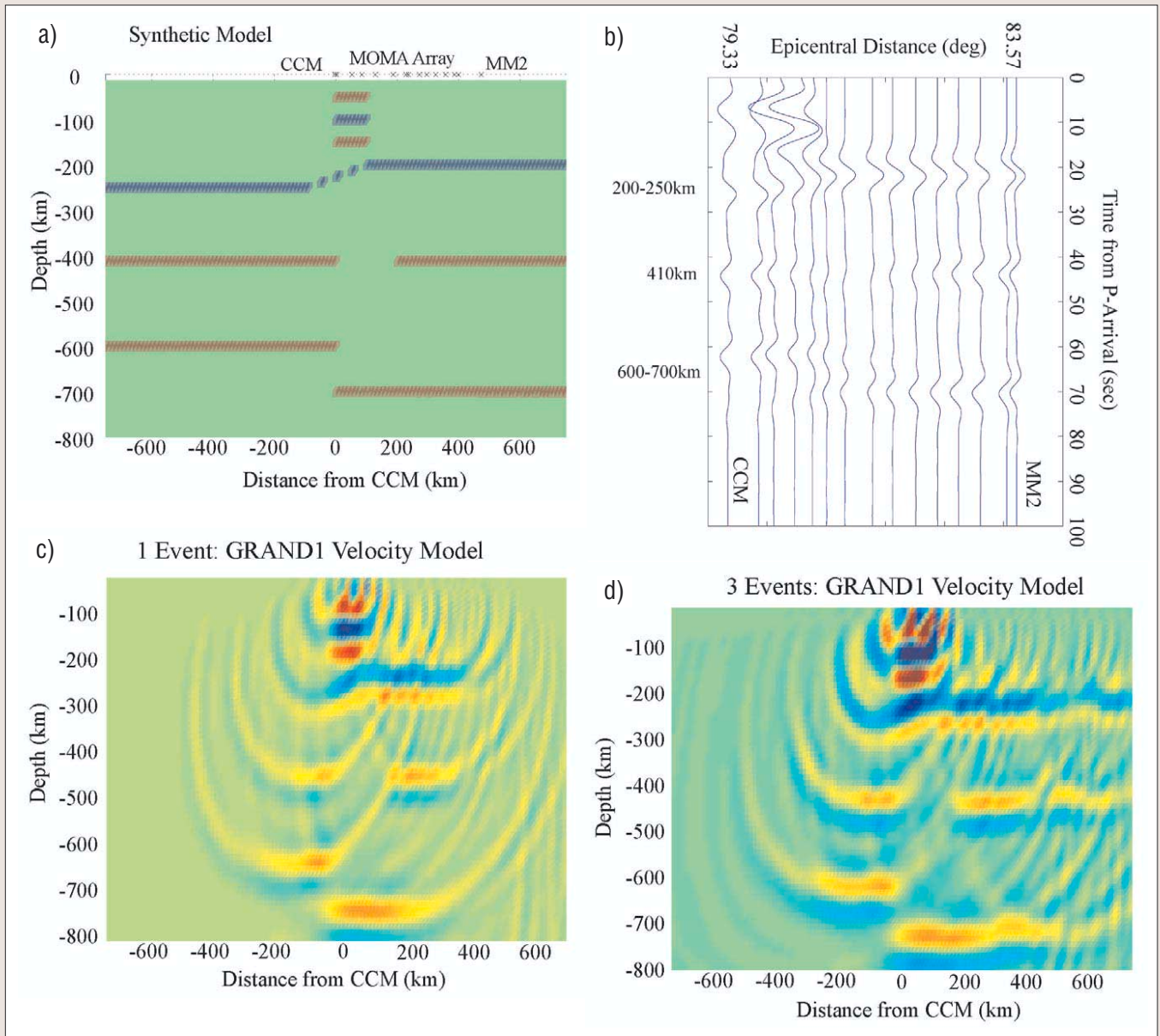


**Figure 4.** Laterally variable test case, in which converters at different depths are embedded in the Grand and Helmsberger shield North America reference model. The receiver array is patterned after part of the MOMA experiment geometry and includes station dropouts. (a) Converter model. (b) Synthetic seismograms for a single source at  $79.3^\circ$  from station CCM, incident from the left. Events from different depths in the model are identified. (c) Reconstructed image from a single event. The imaging region is skewed to the source side. (d) Reconstructed image from four events at variable distances, all incident from the left. Converters are imaged as shallowly as about 100 km with a 6-s pulse.

Under the strictly 1D velocity function assumption, the different azimuths illustrate the effects of different apparent array apertures and apparent station separations on image quality. Northern Pacific earthquakes have azimuths from the northwest and large parts of their upper mantle travel paths are through the Achaean craton. The effective array aperture is 425 km, and the effective station interval is 20 km. South American earthquakes have travel paths through parts of the North and South American cratons. The input signals are turning rays with bottoming points beneath the Caribbean (see Figure 1a). The effective array aperture and station spacing was close to that for the northern Pacific earthquakes. Mediterranean earthquakes arrive from the northeast of the array and have travel paths largely in the oceanic mantle and the eastern edge of the North American continent. The Mediterranean earthquakes are closest to being along the same azimuth as the linear array, and hence produce the largest apparent aperture, 1640 km, and apparent station spac-

ing of 78 km.

The image from the northwest (Figure 5) was made by prestack depth migrating each of six common earthquake gathers and then stacking the images. The image from this azimuth shows clear coherent 410-km and 670-km discontinuities with slight variations in depth. Several shallower coherent events appear at 150 and about 270 km depth. The former is most likely a crustal multiple based on synthetic model studies, whereas the latter has been identified as an upper mantle interface by Li et al.

The image from the southern azimuth was made with four events (Figure 6). The image from this azimuth shows less well developed 410- and 670-discontinuities. The shallower event at 150 is clear, but the deeper 270-km event appears only on the northern edge of the array. The 150-km event again is likely the crustal multiple based on synthetic studies by Li et al. The weakness and limited southern extent of the 270-km event may mark the southeastern edge of the North American craton, in

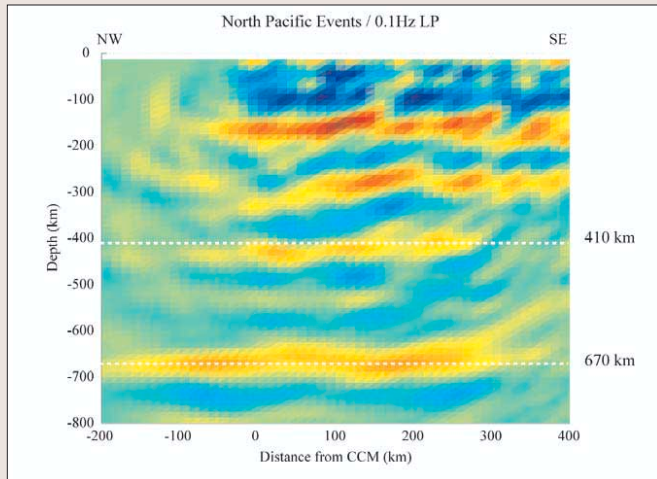


**Figure 5.** Prestack depth-migrated image of MOMA array data. The image was formed by stacking images from signals from six earthquakes at northwestern azimuths. Data were low-pass filtered with a 0.1 Hz corner frequency. The apparent array aperture is 425 km, with apparent station spacing of 20 km. The 410 and 670 discontinuities are clearly imaged. The event at 150 km has been modeled as a crustal multiple by Li et al., whereas the event at 270 km is interpreted as an upper mantle discontinuity.

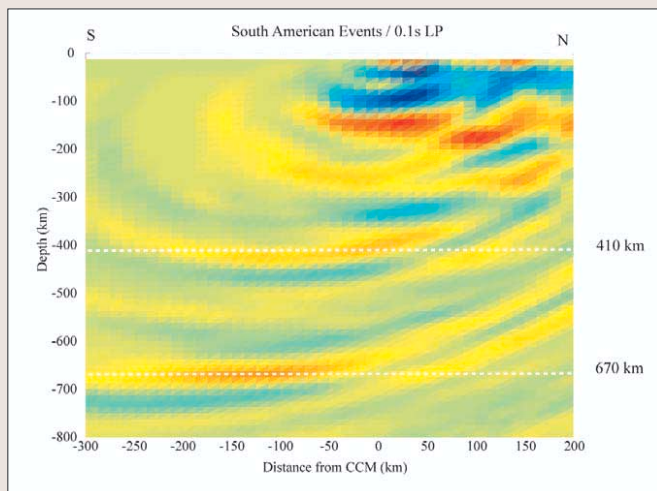


**Figure 6.** Prestack depth-migrated image of MOMA array data. The image was formed by summing images from signals from four earthquakes at southern azimuths. Data were low-pass filtered with a 0.1 Hz corner frequency. The apparent array aperture is 425 km, with apparent station spacing of 20 km. The 410 and 670 discontinuities are well imaged. The event at 150 km has been modeled as a crustal multiple by Li et al. The event at 270 km is truncated beneath the northern edge of the array.

agreement with global tomography (Grand, 1994). Image quality along this azimuth is lower due to fewer events and missing data due to instrument dropouts. Such dropouts are fairly common given the 12-18 month recording times used in passive seismology experiments (see Owens and Fowler in this issue for a discussion of the instrumentation and recording system used).

Figure 7 shows images from three earthquakes from the Mediterranean. The spatial aliasing frequency for imaging at 200 km depth at this azimuth is  $\sim 0.05$  Hz (20 s, Figure 2). The images, made from data low-pass filtered with 0.0667 and 0.05 Hz filter corners, show the effects of inadequate spatial sampling. The 410-km discontinuity appears as a relatively discontinuous event with highly variable strength, an artifact of an undersampled image. The 670-km discontinuity shows greater coherence but similar amplitude variation. The 270-

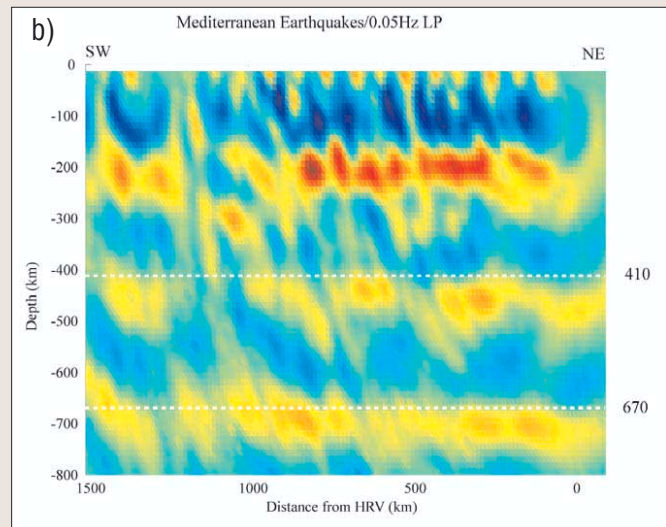
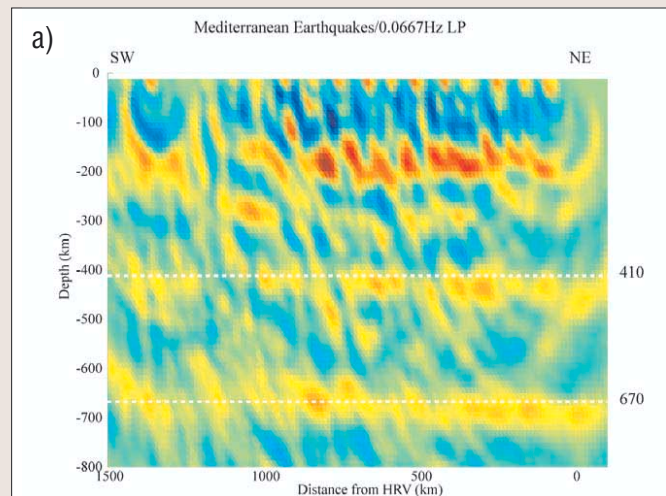


**Figure 7.** Prestack depth-migrated image of MOMA array data. The image was formed by summing images from signals from three earthquakes at east-northeastern azimuths. Data were low-pass filtered with (a) 0.0667 Hz and (b) 0.05 Hz corner frequencies. The apparent array aperture is 1640 km, with apparent station spacing of 78 km. The discontinuity structure is imaged unevenly due to the large station spacing. With the 0.05-Hz filter, the events at 150 km and 270 km are beginning to merge.

km event appears intermittently across the array, and is strongest and most continuous in the center of the array on the 15 s (0.0667 Hz) image.

**Discussion.** The synthetic and data examples illustrate some capabilities of imaging the upper mantle with teleseismic signals using exploration-style depth migration methods. The images were made without any attempt to improve lateral coherence by lateral smoothing either as data preconditioning or postmigration image processing. In the field data case, the images are degraded by assumptions regarding the recording geometry and the seismic velocity model, by ignoring angular variation in conversion strength in the imaging algorithm, by the coarse receiver spacing, and by the small number of earthquake sources. Nonetheless, converted events from the most prominent velocity and density contrasts in the upper mantle, the 410 and 670 discontinuities, are well imaged. Additional conversion events from less globally prominent mantle discontinuities are also imaged, as are crustal multiple reflections. One of the most serious technical problems facing the earthquake imaging community is also one faced by the exploration

community, estimation of the local velocity field for use in migration.

USArray's Bigfoot and Flexible component arrays will be capable of producing significantly higher resolution images in 3D using imaging methods like that applied here. In addition to providing a regular 2D station spacing in Bigfoot, and denser spacing in linear or areal Flexible array deployments, both the arrays will record a far greater number of earthquakes for analysis than were recorded by MOMA. This will result from longer deployment times, more robust instrumentation, and real time telemetry of the seismic data, permitting identification of malfunctioning stations virtually as soon as they fail.

**Suggested reading.** "Preliminary reference Earth Model (PREM)" by Dziewonski and Anderson (*Physics of the Earth and Planetary Interiors*, 1981). "Upper mantle shear structure of North America" by Grand and Helmberger (*Geophysical Journal of the Royal Astronomical Society*, 1984). "Mantle shear structure beneath the Americas and surrounding oceans" by Grand (*Journal of Geophysical Research*, 1994). "The Missouri to Massachusetts Experiment" by Fischer et al. (*IRIS Newsletter*, 1996). "Crust and upper mantle discontinuity structure beneath eastern North America" by Li et al. (*Journal of Geophysical Research*). "Multiparameter two-dimensional inversion of scattered teleseismic body waves; 1, Theory for oblique incidence" by Bostock et al., (*Journal of Geophysical Research*, 2001). "Prestack planewave migration of teleseismic P-to-S converted Phases: Part I, Theory" by Poppeliers and Pavlis (*Journal of Geophysical Research*, in press).

*Acknowledgments: I thank Aibing Li and Karen Fischer for the receiver function data from the MOMA experiment. Much research was done while I was on sabbatical as a Green Scholar at IGPP, Scripps Institution of*

*Oceanography. I gratefully acknowledge support from Scripps.*

*Corresponding author: alan@esci.rice.edu*

**Appendix.** The imaging can be done with a scalar form of the Rayleigh-Sommerfeld diffraction integral, a far field approximation to the Kirchhoff integral that can be expressed in the frequency domain as:

$$I_j(r) = c \int_{-\infty}^{\infty} d\omega \int_{-x_1}^{x_2} dS(r_0) \left[ R_j(r_0, \omega) \left( \frac{\omega}{\beta(r_0)} \right)^{n/2} A_p(r_H, r) A_s(r, r_0) T_{ps}(\theta_{ps}(r)) \cos \theta_s(r_0) \exp(i\omega(\tau_p + \tau_s)) \right]$$

where  $c$  is a constant that accounts for recording geometry and source parameters,  $n$  is an integer that depends on recording geometry,  $r$  is the imaging point,  $r_0$  defines the integration surface  $S$ ,  $\omega$  is angular frequency,  $R_j(r_0, \omega)$  is the receiver function calculated at the  $r_0$  position from the  $j^{\text{th}}$  earthquake,  $A_p(r_H, r)$  is the amplitude correction for the P-wave from the hypocenter to the scattering point,  $A_s(r, r_0)$  is the amplitude correction for the scattered S-wave to the Earth's surface, and  $T_{ps}(\theta_p(r), \theta_s(r))$  accounts for angular variation of P to S conversion at scattering point  $r$ .

$\beta(r_0)$  is the shear velocity at the surface,  $\theta_s(r_0)$  is the incidence angle of the scattered S wave at the surface,  $\theta_{ps}(r)$  is the scattered S wave angle relative to the input P wave angle at the scattering point,  $t_p(r_H, r)$  is the travel time of the P wave from the source to the scattering point, and  $t_s(r, r_0)$  is the travel time of the scattered S wave to the surface.

The final image volume is the stack over all earthquakes,  $m$ ,

$$I(r) = \sum_{j=1}^m I_j(r) \quad \cdot \quad \text{TJE}$$